Aalborg Universitet

AALBORG
UNIVERSITY

Towards 6G in-X subnetworks with sub-millisecond communication cycles and extreme reliability

Adeogun, Ramoni; Berardinelli, Gilberto; E. Mogensen, Preben; Rodriguez, Ignacio; Razzaghpour, Mohammad

Link to publication from Aalborg University

Towards 6G in-X Subnetworks With Sub-Millisecond Communication Cycles and Extreme Reliability

RAMONI ADEOGUN[1], **(Senior Member, IEEE), GILBERTO BERARDINELLI**[1], **(Member, IEEE),**
PREBEN E. MOGENSEN[1,2], **IGNACIO RODRIGUEZ**[1], **(Member, IEEE),**
AND MOHAMMAD RAZZAGHPOUR[1], **(Member, IEEE)**

[1]Department of Electronic Systems, Aalborg University, 9220 Aalborg, Denmark
[2]Nokia Bell Labs, 9220 Aalborg, Denmark

Corresponding author: Ramoni Adeogun (ra@es.aau.dk)

ABSTRACT The continuous proliferation of applications requiring wireless connectivity will eventually result in latency and reliability requirements beyond what is achievable with current technologies. Such applications can for example include industrial control at the sensor-actuator level, intra-vehicle communication, fast closed loop control in intra-body networks and intra-avionics communication. In this article, we present the design of short range Wireless Isochronous Real Time (WIRT) in-X subnetworks aimed at life-critical applications with communication cycles shorter than 0.1 ms and outage probability below 10^{-6}. Such targets are clearly beyond what is supported by the 5th Generation (5G) radio technology, and position WIRT as a possible 6th Generation (6G) system. WIRT subnetworks are envisioned to be deployed for instance in industrial production modules, robots, or inside vehicles. We identify technology components as well as spectrum bands for WIRT subnetworks and present major design aspects including frame structure and transmission techniques. The performance evaluation considering a dense scenario with up to 2 devices per m^2 reveal that a multi-GHz spectrum may be required for ensuring high spatial service availability. The possibility of running WIRT as an ultra-wideband underlay system in the centimeter-wave spectrum region is also discussed. Aspects related to design of techniques for the control plane as well as enhancements to the presented design is the focus of our ongoing research.

INDEX TERMS URLLC, intra-vehicular communications, Industry 4.0, beyond 5G, 6G, sub-millisecond cycle, short-range, in-X subnetworks, intra-avionics.

I. INTRODUCTION

Wireless communication is identified as a major enabler of the Industry 4.0 vision [1], aiming at enhanced productivity via dynamic allocation of production resources, agile scalability, improved efficiency and flexibility [2]. Industrial wireless networks are expected to replace the bulky wired infrastructure of traditional industrial networks such as Ethercat [3], Profinet [4], [5] or the set of Time sensitive Networks (TSN) solutions [6], enabling the control of mobile and reconfigurable cyber-physical systems.

The nature of the industrial control traffic leads in some cases to stricter requirements in terms of latency and relia-

bility than typical broadband traffic, characterized by greed of high data rates with non-strictly bounded delays. Communication latencies in industrial control networks range indeed from seconds (for operations such as plant asset management and traffic control) down to milliseconds (ms) or fraction of ms for fast closed loop control at sensors-actuators level [7]. Similarly, the reliability requirement (usually defined in terms of packet loss rate within the tolerated delay) can approach in the most demanding cases extreme levels in the order of 10^{-6} to 10^{-9}, for the sake of preserving the stability of the control loop. From a communication perspective, closed loop control features a specific type of traffic, referred as *isochronous*, characterized by periodic transmission of measurements and control commands with strictly limited jitter tolerance.

The associate editor coordinating the review of this manuscript and approving it for publication was Cesar Briso.

The automotive industry is also witnessing dramatic increase in the number of sensors requiring connectivity which has resulted to a surge in the demand for fast and flexible wireless communication technologies to be installed within vehicles [8]. Wireless is expected to replace wired or fiber solutions such as Controller Area Network (CAN) for body control data exchange, Local Interconnect Networks (LIN) for exchanging small serial control messages, and Media Oriented Systems Transport (MOST) for infotainment data transmission [8], and has the advantage of eliminating the costs associated to cables installation and maintenance. The support of life critical in-vehicle operations such as ignition, suspension and brake control will require extremely reliable connections.

A. EXISTING TECHNOLOGIES

Major efforts in both industry and academia are spent on the design of wireless solutions to be adopted in such setups. Most of the solutions designed for industrial control in the last decade are built upon existing radio standards such as IEEE 802.15.1, 802.15.4 [9] or 802.11 [10] with customized upper layers for improving robustness to radio impairments such as interference and frequency-selective fading. For example, Wireless Interface to Sensors and Actuators (WISA) is based on the physical layer of IEEE 802.15.1 with an enhanced frequency hopping scheme for harvesting diversity gains [11]. Similarly, WirelessHART uses the IEEE 802.15.4 physical layer and introduces new data link, network, transport and application layers that capitalize from a centralized scheduler [12]. Other relevant examples of wireless industrial technologies are ISA 100.11a [13], WIA-PA [14], WIA-FA [15]. Given their dependency on physical layer standards designed for other purposes, such technologies have however inherent design limitations which impede them to achieve the low latencies demanded by the most challenging industrial applications [16]; further, they operate in the crowded 2.4 GHz unlicensed spectrum where interference is a major limiting factor for achieving high reliability.

Cellular technologies such as Long Term Evolution (LTE) [17] have obvious advantages in terms of reliability given the usage of licensed spectrum, but lead to the necessity of establishing a contract with a mobile operator and pay out connectivity as a service. Furthermore, the minimum transmission time unit, known as Transmission Time Interval (TTI), in LTE is set to 1 ms; this may also prevent the usability of such technology for closed loop control with very short cycles. The 3rd Generation Partnership Project (3GPP) has finalized in 2018 the specifications for the 5th Generation New Radio (5G NR) standard [18], also indicated as Release 15 (Rel-15), which includes the support of ultra-reliable low latency communication (URLLC) service class defined by the International Telecommunication Union (ITU), and targeting 1 ms latency with a 10^{-5} reliability [19]. Such targets are achieved by introducing the concept of *mini-slot*, i.e., TTI with significantly shorter duration than the 1 ms one in previous LTE releases, as well as by including the

options of larger subcarrier spacings, optimized grant-free access procedures [20] and pre-emptive scheduling mechanisms [21]. Current research on Release 16 (Rel-16) aims at extending the previous release with the support of different frequency bands, including unlicensed spectrum, as well as integrating the wireless 5G system with wired TSN solutions, the latter concept known as Time Sensitive Communication (TSC) [22].

5G NR definitely represents a leap in performance towards URLLC with respect to other existing radio technologies. Nonetheless, communication at sensors and actuators level may feature cycle time down to fraction of ms and therefore significantly below the URLLC target defined by ITU. Examples of use cases demanding such fast communication cycles can be the aforementioned intra-vehicle communication for engine and suspension control [23], drive control of robotic manipulators, power system protection and power electronics control [16]. These use cases reflect scenarios with short communication range, not larger than a few meters, but with requirements of extreme reliability for preserving the stability of the control loop.

Extreme reliability with fraction of ms communication cycles has already been identified as a relevant research objective for upcoming 6th Generation (6G) radios [24], but related research is still at its infancy. In [25], a new physical layer numerology aimed at reducing the control overhead and transmission time of IEEE 802.11 radio standard is proposed. The numerology enabled the support of transmissions with cycle times down to 0.1 ms. However, reliability aspects are not discussed in detail. In [26], we have justified the need for a novel Wireless Isochronous Real Time (WIRT) system aimed at 0.1 ms cycles and wired-like reliability. We discussed possibilities of WIRT operation over the centimeter-wave and millimeter-wave spectrum regions. A discussion on usage of short range 6G subnetworks with super-fast communication cycles and extreme reliability in life critical applications is presented in [27].

B. CONTRIBUTIONS

In this article, we present a comprehensive discussion on the initial design for such short range WIRT system. We conceive WIRT cells as *subnetworks*, which can be integrated with existing cellular infrastructure for the sake of offloading it from the most challenging services, but are also expected to provide the same service level even when out of coverage of external infrastructure. WIRT subnetworks can be installed in a plethora of new scenarios, such as in robots, in production modules, in vehicles, in aircrafts, and even in human bodies. In that respect, we refer to WIRT subnetworks as *in-X* subnetworks. Potential bands and main technology enablers are presented, along with a description of a possible frame structure and numerology configurations. In particular, we investigate the required bandwidth for achieving sub-ms extremely reliable communication cycles in dense scenarios via a semi-analytical system evaluation analysis. Our design is in principle clean slate, i.e. without concerns of
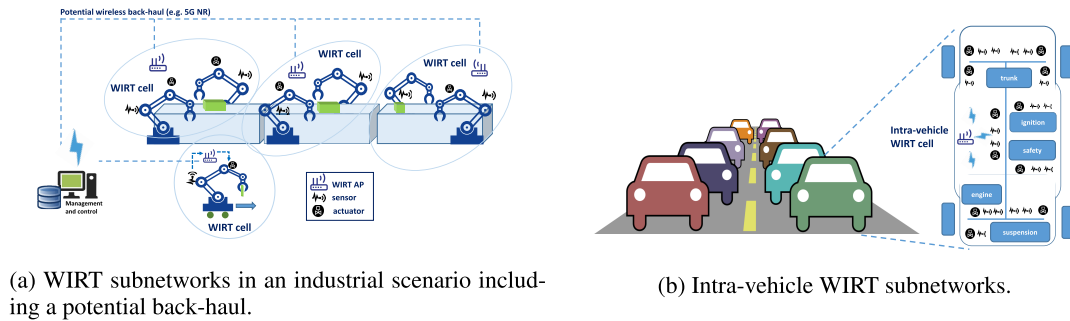
(a) WIRT subnetworks in an industrial scenario including a potential back-haul.

(b) Intra-vehicle WIRT subnetworks.

FIGURE 1. Possible WIRT scenarios.

backward compatibility with existing 5G releases, though the possibility of evolving the latter to the new targets is also discussed. Aspects related to both generated and received interference are presented, together with potential enhancements for loaded scenarios.

The sub-ms cycles and the extreme reliability clearly positions in-X WIRT subnetworks beyond what is supported by 5G NR, and therefore as a potential upcoming 6G system.

To sum up, the main contributions of this article are the following:

- We present a potential design of a novel radio system for the support of isochronous real time traffic for closed loop control, whose cycle times are a factor of $\sim \times 10$ shorter than the latency targets of existing radio technologies (i.e., ≤ 0.1 ms).
- We estimate the required bandwidth for achieving such short cycles with extreme reliability in potentially dense scenarios, and subsequently identify possible spectra where WIRT subnetworks are to be deployed, with focus on the below 10 GHz centimeter-wave spectrum region.
- We identify possible viable enhancement for reducing the required bandwidth and/or increasing the number of supported control loops at a given bandwidth.

To the best of the authors' knowledge, this is the first article addressing in detail the problem of wirelessly supporting control cycles of a fraction of ms and extreme reliability in potentially ultra-dense deployments.

The remaining part of the article is structured as follows: Section II presents our general vision for WIRT in-X subnetworks. In Section III, we identify potential spectrum options for WIRT deployment. A comprehensive discussion of the system design is then presented in section IV followed by description of the methodology for evaluating WIRT performance in Section V. The evaluation results as well as discussion of their implications for WIRT deployment are presented in Section VI. Finally, we draw conclusions in Section VII.

II. WIRELESS ISOCHRONOUS REAL TIME SYSTEM

We conceive WIRT as a system composed of short-range radio subnetworks for supporting fast closed loop control. Each WIRT subnetwork corresponds to a short range (not larger than 10 m) low-power cell installed at a specific location in scenarios such as modules of an assembly line, or articulated mobile robots, or inside a vehicle or aircraft. Such subnetworks can also be used in intra-body communication for monitoring the occurrence of physical anomalies which require immediate actions that can not be left to an external processing unit. For instance, WIRT subnetworks can be used as an enabler for a wireless cardiac pacemaker for regulating heartbeats in patients with abnormal rhythm [27]. In general, a WIRT subnetwork can be installed in any entity requiring local control of its operations. This eases the support of life-critical services with respect to a scenario where operations are controlled by an external micro/macro cell, and are therefore more prone to possible coverage holes. As a consequence of the low power, short range subnetworks enable aggressive spectrum reuse, and therefore an improved resource efficiency relative to micro-cells operating at a higher power [28]. Figure 1 depicts two possible installations for WIRT in-X subnetworks, considering an industrial setup or the intra-vehicular use cases.

The target of the WIRT design is to achieve cycle times below 0.1 ms and extremely high reliability ($10^{-6} - 10^{-9}$) for a large number of devices. Recent 3GPP specifications addressing industrial scenarios consider device densities in the order to 100,000 per km^2 (i.e., 0.1 per m^2) for motion control applications with production cells of size 10m $\times$ 10m [29], though considering communication cycles of a few ms. However, future Industry 4.0 scenarios may feature smaller and interchangeable production cells or robots, besides coping wirelessly with more stringent communication cycles. Also, for intra-vehicle communications, the number of sensors per vehicle is expected to be up to 200 in the coming years [30], though only part of the associated control loops may target sub-ms cycles. To the best of the authors' knowledge, requirements for device densities targeting sub-ms cycles for industrial and/or intra-vehicle communication have not been defined yet by standardization bodies. In order to verify the capabilities of the WIRT systems to operate in harsh conditions, we therefore focus on challenging cases with significantly higher device densities than what is targeted by 3GPP [29], e.g., 2 devices per m^2. Similarly, scenarios characterized by unprecedented cell densities can appear,

e.g., vehicles in a congested road in which each vehicle is equipped with a WIRT subnetwork. While 5G ultra-dense deployments consider a maximum density of $\sim$2500 base stations per km^2 [31], we consider a cell density of at least a factor of $\sim \times 10$ above, i.e. 25000-40000 cells per km^2 for WIRT and leave characterization of expected scenario-specific cell densities for future work.

Also, we aim at a scalable design where more relaxed cycles (e.g., ms or above) can also be supported in the same air interface; a WIRT subnetwork may indeed need to serve control loops with different cycle duration and reliability targets. The achievement of the tighter requirements poses obvious challenges for physical layer and medium access control design. Also, interference may become a major limiting factor in scenarios characterized by high cell and device density. Since operations of WIRT subnetworks can be life-critical, their tight packet loss requirements must be achieved virtually everywhere, regardless of interference and radio propagation conditions.

Operations of WIRT subnetworks can be independent or coordinated via a back-haul communication link. Intra-vehicle subnetworks are likely to be independent due to the difficulty of coordinating operations with subnetworks installed in neighbor vehicles, whose position is not known beforehand and varies over time. Indoor factory scenarios with controlled assets can instead support coordinated deployments. In [26], we presented a possible system architecture where multiple WIRT subnetworks are connected via a 5G NR network, that can guarantee reliable communication with a few ms latency over hundreds of meters range. Such a network can for example be used for controlling the operations of a set of robots which can be instructed to perform specific operations such as drilling, assembling, or moving in the production area without collision, while WIRT subnetworks installed in robots or production modules focus on the short range fast control such as as drive control (e.g., control of arm, wrist, body, joint rotation, or grippers). Also, back-haul network can in principle enable coordination of the radio resources (e.g., time slots and/or frequency channels) among the WIRT subnetworks in order to minimize mutual interference.

Each WIRT subnetwork consists of a controller acting as an access point for a number of sensors and actuators as illustrated in Figure 2. Sensors are periodically transmitting measurements to the controller, while the actuators are receiving periodic commands from the controller. These commands are calculated upon processing of the sensors' measurements. By using digital communication jargon, we assume that both measurements and commands are mapped to a transmission packet. A WIRT controller can be associated to a single sensor - actuator pair, or to a group of sensors and actuators; in the latter case, it collects measurements from multiple sensors and map them to a single or multiple packets. Similarly, the controller can map a command to a single packet for a specific actuator, or multiple commands to multiple actuators. Though the data plane is unidirectional,
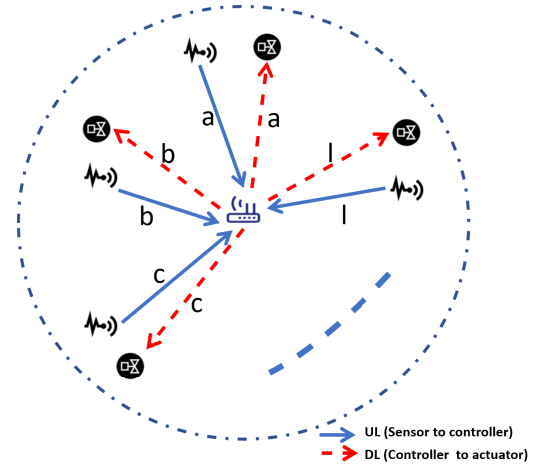

FIGURE 2. A WIRT cell with 12 sensor-actuator pairs. *a,b,c,…,l* denote the pairs.

a bi-directional control plane is needed for connection establishment and maintenance. This would be further described in Section IV.

It is worth to mention that the entire processing for issuing commands to the actuators needs to be performed locally at the controller. Considering the super-short cycle time, the possibility of moving the processing to an edge cloud is not considered since it would introduce extra delays which may severely limit the achievable latencies. However, in cases (e.g., industrial set-up) where connection of the WIRT controller to the external internet or to a common wireless infrastructure for the subnetworks is possible, the WIRT controller can also act as a gateway for delay-tolerant applications. Thus, the controller can periodically (at significantly larger intervals than the actual control operations) transfer data gathered at each subnetwork to an edge cloud which can then use it for analytics or predictive maintenance.

The scenarios where WIRT systems are expected to be used can include mobile subnetworks (e.g., WIRT cells in a vehicle, robots, or inside human-body). For these use-cases, it is unlikely that devices (sensors and actuators) will move away from the controller beyond a maximum cell radius of 10 m. We therefore assume each device to be served by a single controller for the whole operation time, without the option of handing over communication to other subnetworks. Note that, in life-critical scenarios, a WIRT installation should guarantee the necessary equipment redundancy for fault tolerance. For example, multiple controllers can be installed within a single subnetwork to accommodate potential controller faults. In the case of a fault of the serving controller, its operations must be seamlessly transferred to another controller within the subnetwork.

III. SPECTRUM OPTIONS FOR WIRT
As identified in [26], support of communication cycles in the order of a fraction of ms with wired-like reliability leads to a large bandwidth requirement and raises the immediate

question on the spectrum region where WIRT could be deployed. Millimeter-waves [32], [33] and, recently, Tera-Hertz bands [34] have attracted tremendous attention by both industry and academia given the availability of a large spectrum, which can support a variety of broadband services and challenging low latency applications including the WIRT short communication cycles. Propagation at these frequencies is however challenging due to cumbersome losses as compared to the lower frequency bands, and further research is needed in order to asses their suitability for WIRT.

In this article, we restrict our focus to the below 10 GHz centimeter-wave spectrum options for WIRT. The immediate advantage of focusing on such spectrum region is the possibility of exploiting the domain knowledge of most of the existing radio technologies, that are operating in this range. On the other side, such spectrum is largely populated and this may pose a challenge towards ensuring sufficient amount of available spectrum for WIRT.

A number of bands in the sub-6 GHz spectrum (denoted as Frequency Range 1 (FR1)) have been specified for 5G NR, covering the interval 1.7 GHz to 4.7 GHz, with a maximum contiguous spectrum size of 100 MHz [35]. Particularly interesting is the so called *mid-band* located in the 3.4 GHz-3.8 GHz region where diverse policies of usage are emerging on a regional basis [36]. In USA, the 3.5 GHz band is known as Citizens Broadcast Radio Service (CBRS), with 150 MHz available spectrum, used for radar systems but now also available for commercial use based on a temporary license and a dynamic spectrum access scheme [37]. Such shared-basis approach is expected to ease the deployment of local 5G networks since individual and costly spectrum licences are not to be acquired [38]. Still, the usage of the 3.5 GHz band may require the service to be provided by a mobile operator, and a fee to be paid on an ongoing basis.

License-exempt bands eliminate the burden of relying on an external actor for connectivity services. However, the reliability of a system operating in the unlicensed spectrum may be affected by the interference from potential coexisting radio systems.

When focusing in the below 10 GHz spectrum region, the obvious candidate unlicensed bands are the 2.4 GHz and 5 GHz bands. Bands in the below 1 GHz spectrum such as the 868 MHz or 915 MHz bands used for Low Power Wide Area Network (LPWAN) [39], [40] are indeed to be discarded beforehand given their limited size. The 2.4 GHz band is still rather narrow (∼83 MHz) and extremely crowded [41]. The 5 GHz band is fragmented in several chunks with different regional regulations on channel access mechanisms [42], [43]. Though its current usage is rather low relative to the 2.4 GHz band, it is foreseen to increase dramatically in the coming years [44]. Moreover, both the US Federal Communications Commission (FCC) and European Telecommunications Standards Institute (ETSI) require a Dynamic Frequency Selection (DFS) mechanism to run at each device in the ranges 5.250 GHz - 5.350 GHz and 5.470 GHz - 5.725 GHz for avoiding interference with radar

systems operating in the same bands. Also, a Clear Channel Assessment (CCA) procedure via Listen Before Talk (LBT) is required for most of the available bands. This requirement leads to significant delays and idle periods that compromise the possibility of achieving low latency. Such procedures are meant to avoid greedy user behaviors and ensure a fair medium sharing but are in contrast with our need of periodic access.

Recently, FCC has promoted additional spectrum for unlicensed usage in the 5.925 GHz - 7.125 GHz range. This is commonly referred to the 6 GHz band, and its regulations are currently been defined. The current trend of extending the availability of unlicensed access, even in the below 10 GHz spectrum region, copes with the necessity of dealing with the spectrum crunch due to the exponential increase of wireless applications. Unlicensed access also eliminate the obsolete licensing paradigm, which is known to lead to inefficient spectrum utilization [45].

Obviously, the presented options lead to exploitable bands of different sizes and subject to different regulations. It is clear that regulatory mechanisms other than CCA should be applied in case low latency applications are to be deployed over unlicensed spectra. For example, restrictions on power spectral density are more suited for WIRT since they do not affect the periodicity of the transmission but only communication range and/or overall transmission time for each sensor.

In Section VI, we will estimate the required bandwidth for supporting the challenging WIRT requirements in a dense network, and discuss the possibility of operating WIRT as an underlay system over bands potentially occupied by other radio systems.

IV. SYSTEM DESIGN

In this section, we present a potential design for WIRT based on the technology enablers identified above. We describe a possible medium access design and highlight the possibility for supporting cycles shorter than 0.1 ms using Orthogonal Frequency Division Multiplexing (OFDM) modulation.

A. TECHNOLOGY ENABLERS

In [26], we identified the following main technology enablers for the wireless support of isochronous real time transmission:

1) Periodic transmissions with tight jitter control over a set of pre-allocated and dedicated frequency resources at each device in a subnetwork.

2) Blind repetitions of the same robustly coded packet to be completed within a short time interval. We note here that the repetitions may be redundant in cases with successful prior transmission resulting in poor spectral efficiency. This is however inevitable for ultra reliable communication with low latencies. For instance, in [46], URLLC targeting 1 ms latency with grant free transmission in 5G NR was shown to result in a spectral efficiency loss up to a factor of ×10 relative to best effort mobile broadband. It is worth mentioning that
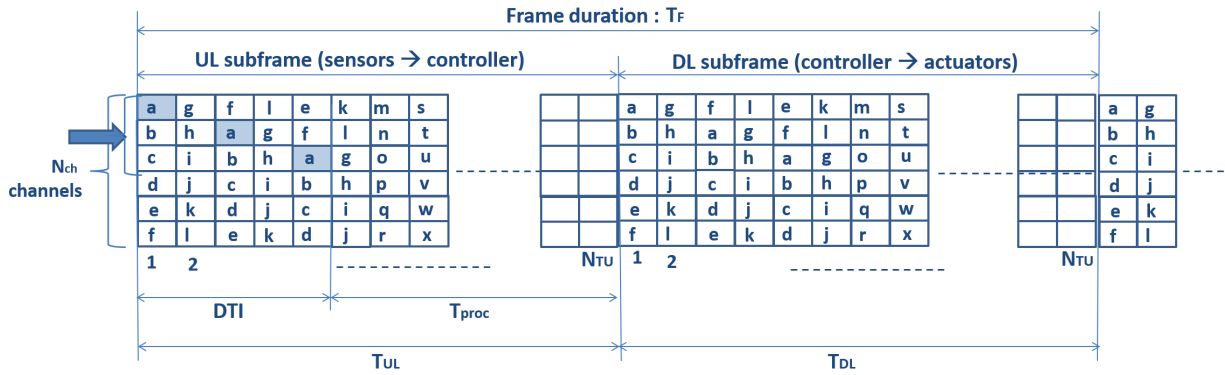
FIGURE 3. Example of frame structure with symmetric UL and DL. *a,b,c,...* denotes specific communication loops which are illustrated in Figure 2. N_{ch} = 6 channels and N_{rep} = 3 repetitions are assumed. DTI, N_{TU} and T_{proc} denote the device transmission interval, number of transmission units per subframe and processing time available to the controller, respectively.

a packet repetition scheme has advantages in terms of implementation complexity with respect to a single transmission at a lower coding rate, since it reduces the required buffer size at the receiver.

3) Large frequency diversity to be achieved by hopping each of the blind repetitions over different frequency channels. Hopping patterns used by devices in a sub-network are to be orthogonal to avoid collisions.
Channel hopping also allows randomizing the impact of inter-cell interference, provided devices in neighbor subnetworks operate with different hopping patterns. Hopping over different channels at each repetition can indeed limit the risk that the same interferers are active at the same time over the same channels repeatedly, thus achieving interference diversity. It should be noted that the anti-interference and security features of frequency hopping have been successfully exploited in other wireless technologies for both military and civilian applications [47].

B. MEDIUM ACCESS

We present a design for Time Division Duplex (TDD) mode. Such duplexing mode eases the deployment over different spectra with respect to Frequency Division Duplex (FDD) mode, where paired bands are required for uplink (UL) and downlink (DL) transmissions, respectively [48]. TDD mode results then in a more efficient spectrum utilization due to usage of single frequency channel and elimination of the channel separation requirement in FDD. Moreover, TDD devices benefit from lower cost since no duplexer is needed to isolate UL and DL transmissions [49]. We believe such benefits are predominant with respect to the inherent delay penalty due to the fact that UL and DL transmission can only happen sequentially, since the latter can be counteracted via proper system and numerology design.

A possible frame structure aiming at supporting WIRT traffic is depicted in Figure 3. The frame is divided in an UL and a DL subframe of duration T_{UL} and T_{DL}, respectively,

where the UL refers to the communication link between sensors and controllers, and DL to the communication link between controllers and actuators. Each sensor (or group of sensors) reports measurements at a sampling interval equal to the frame duration $T_F = T_{UL} + T_{DL}$. Similarly, the actuators expect to receive commands at intervals T_F. We refer to a *loop* as the ensemble of UL and DL transmission related to a sensor(s)-actuator(s) pair involved in a control action.

The data plane is unidirectional, while a bidirectional control plane is needed in order to establish connection, signal the relevant communication parameters, and eventually correct timing and jitter. A set of radio resources in the frame should then be accommodated to support such procedures. In a ramp-up phase, sensors can acquire the frame timing by receiving the DL reference signals sent by the controller, and transmit their connection requests over a predefined set of UL frequency resources dedicated to connection establishment. Upon reception of connection request, the controller should verify the possibility of ensuring the required time and frequency resources for this control loop, and eventually signal it in the DL over another set of pre-allocated resources. Also, control signaling over UL and DL can enable link adaptation procedures. For the rest of the section, we focus on the data plane while the design of control resources and their appropriate mapping into the frame structure constitutes part of our ongoing research.

The ratio between UL and DL subframe duration depends on the type of control loop. For example, in case multiple sensors report measurement to be used for issuing a command to a single or a lower number of actuators, the UL subframe should be longer than the DL subframe. TDD mode offers an inherent flexibility for adapting to asymmetric traffic with respect to FDD mode, where the paired UL and DL bands are predefined [50]. We focus here on the symmetric UL/DL case, i.e. $T_{UL} = T_{DL}$, reflecting the case with equal number of sensors and actuators.

As suggested in [51], we define the cycle time as the time interval starting from the transmission of a packet from

all the pool of sensors till the reception of the commands issued by controller to all actuators. Thus, the cycle time corresponds to the frame duration. Observe that this definition does not include the processing time for packet generation and command processing at the sensor and actuator, respectively.

Each subframe is divided into N_{TU} transmission units (TUs) where multiple devices can be frequency multiplexed over up to N_{ch} channels. A TU can be seen as the continuous transmission time over a specific frequency channel from a sensor or to a specific actuator. We assume that controllers and sensors transmit a packet over a TU, and repeat its transmission for multiple TUs over different channels. While the presented frame structure in Figure 3 assumes equal payload sizes (and hence, TUs with equal duration) for all sensor-actuator pairs, the structure can be easily adapted to support cases with different packet sizes. For example, a TU can be longer or shorter for a group of channels, such that smaller or larger packets can be mapped over them at parity of spectral efficiency. This may pose some restriction to the channel hopping scheme, i.e. hopping might only be possible over channels whose TU duration is sufficient for its packet size. Another possibility is to maintain the same TU duration for all channels, but vary the channel size. Similarly, the hopping should only happen over channels having the required size.

Transmissions from/to a device are then hopping over n_{ch} channels out of the pool of N_{ch} channels, with $n_{ch} \leq N_{ch}$. Channel hopping allows for operating over a large band, thus achieving frequency and interference diversity, while maintaining a limited instantaneous bandwidth. This translates to a lower chip cost than a wideband transceiver, but assumes the usage of a frequency synthetizer which is able to switch across different subbands [52].

The receiver can process the packet transmitted over the first TU, and only process repetitions in case of failure. We assume the packet repetitions of multiple devices to be time-interleaved on a TU-basis; this is meant to leave sufficient time margin for the frequency synthetizer to hop over a different band, and allows avoiding the insertion of a time gap for such margin in the frame structure.

We define as Device Transmission Interval (DTI), the overall time period for transmitting a packet, including repetitions. A DTI can be assigned to a sensor in the UL and for communication to an actuator in the DL. Observe that the DTI is a device-specific parameter, and DTIs are staggered among different devices. In the example in Figure 3, the DTI of sensor *a* includes TUs 1-5, while the DTI of sensor *g* includes TUs 2-6. The maximum processing time allocated to the controller is, therefore, given by $T_{proc} = T_{UL} - T_{DTI}$, where T_{DTI} denotes the DTI duration. Note that the controller processing time after each sensor transmission includes both the time for detection of the received packet and associated operations for issuing the appropriate command(s) to the actuator.

In order to avoid collisions, devices within a WIRT subnetwork are allocated specific orthogonal hopping patterns. In Figure 3, it is assumed that, given the UL/DL symmetry, the same pattern used by a sensor in the UL is applied to issue the command to a corresponding actuator in the DL. This symmetry allows preserving the same T_{proc} for all the communication loops, regardless of their position in the UL/DL subframe. It can be shown (proof in Appendix) that the maximum number of supported communication loops is given by

$$N_L = \left\lfloor \frac{N_{TU}}{2N_{rep}} \right\rfloor 2N_{ch} + \left\lfloor \frac{N_{TU} - \left\lfloor \frac{N_{TU}}{2N_{rep}} \right\rfloor 2N_{rep}}{2N_{rep} - 1} \right\rfloor N_{ch}, \quad (1)$$

where N_{rep} is the number of packet repetitions (including the case of single transmission, i,e., $N_{rep} = 1$), and $\lfloor x \rfloor$ denotes the greatest integer less than or equal to x. Note that, since each repetition is expected to happen over a different channel, the maximum number of repetitions is equal to the number of used channels, i.e., $N_{rep} = n_{ch}$. This also implies that the number of repetitions needed for harvesting frequency and interference diversity is limited by the number of available channels, N_{ch}, and hence, by the available bandwidth.

Observe that, while in the UL each device is transmitting over a time interval T_{DTI} (including the intervals for hopping), in the DL the controller transmits over an entire subframe. Also, the instantaneous bandwidth of the controller should be as large as the N_{ch} channels since it may need to serve multiple frequency multiplexed actuators simultaneously. The controller, therefore, requires a more complex wideband transceiver than the sensors and actuators, which can operate over a smaller bandwidth and with a single frequency synthetizer combined with hopping. An alternative to a wideband transceiver at the controller could be the usage of multiple narrowband transceivers operating simultaneously over a smaller bandwidth. The design presented here can scale to different cycle times by changing the frame duration, T_F. In the case of a subnetwork supporting cycles with different durations, T_F can instead be set according to the shortest cycle and more relaxed cycles with durations equal to multiple of T_F can be supported by interleaving UL/DL transmissions across multiple packets, or operating at a lower rate.

Orthogonal Frequency Division Multiplexing (OFDM) waveform can be used in WIRT as it benefits from low complexity for signal generation and detection [53], and for such reasons is also currently adopted by several broadband radio standards such as IEEE 802.11, LTE and 5G NR [54]. Subcarrier spacing, Δf, is an important parameter in OFDM design since it defines the duration of the multi-carrier symbol, and therefore, affects its robustness to frequency selective fading, hardware impairments and Doppler spread [55]. In WIRT, a TU can be mapped over a single OFDM symbol. In case the frame is expected to support a large number of devices and therefore includes a large number of TUs within

TABLE 1. WIRT system design.

General characteristics
- Low power small cells, < 10 m range   - Operations in the below 10 GHz centimeter-wave spectrum region   - Support of closed loop control, with cycles time down to 0.1 ms and $10^{-6} - 10^{-9}$ reliability   - Support of potentially dense deployments   - No device mobility across different subnetworks
Technology enablers
- Periodic transmissions with pre-allocation of radio resources, and tight jitter control   - Short transmission intervals with robustly coded packets, and multiple packet repetitions within the transmission interval   - Hopping over different sub-bands for each packet repetition, for harvesting both frequency and interference diversity   - Orthogonality of device transmissions within a subnetwork
Proposed design
- TDD mode, ensuring flexibility to asymmetric traffic (e.g., larger number of sensors than actuators)   - OFDM as a possible waveform   - Scalable frame size, with maximum duration lower than 0.1 ms   - Numerology with large subcarrier spacings (>120 kHz), designed for supporting a large number of control loops and leave sufficient processing margin at the controller   - Interleaved transmission of packet repetitions for enabling sub-band switching

a 0.1 ms cycle, OFDM symbols are to be very short and a large subcarrier spacing is to be used, e.g., >120 kHz. A summary of the general characteristics of a WIRT system, along with technology enablers and design features is reported in Table 1.

V. EVALUATION METHODOLOGY

In this section, we develop a semi-analytic procedure for evaluating the capability of the frame structure and technology enablers presented in Section IV for supporting ultra-reliable short communication cycles in a dense network of WIRT subnetworks. It is worth to mention that, it is not the object of this article to provide a highly realistic system analysis of dense WIRT subnetworks, which will only be possible when the entire design (including control plane, channel coding, signal processing) is in place. We rather aim at obtaining insights on the order of magnitude for the required spectrum, as well as on the impact of relevant features such as packet repetitions and spatial diversity.

A. SCENARIO MODEL

Let us consider a deployment comprising of M subnetworks with N sensor-actuator pairs per cell. The devices in each subnetwork are connected to a dedicated controller located at the center of the subnetwork. Each pair of sensor and actuator is involved in a communication loop, i.e. each subnetwork supports N communication loops. For simplicity, we assume sensor and actuator in a pair to be co-located. As described in Section IV, devices in a subnetwork are assigned orthogonal sets of radio resources. We assume no coordination among the subnetworks and hence, the subnetworks are not synchronized. The subnetworks operate over the same frequency resources and can then generate mutual interference. This can represent real-world cases such as a factory scenario where WIRT subnetworks are installed over production modules or robots, with no back-haul connection enabling

coordinated operations, or an intra-vehicle scenario in a congested road.

Each communication link between sensor-controller and controller-actuator experiences frequency selective fading, and interference from neighbor subnetworks, which can affect the possibility of achieving a desired outage probability target $P_{\text{out},T}$. We assume that a communication loop is successful, if both paired sensor-controller (UL) and controller-actuator (DL) links cope with $P_{\text{out},T}$. A loop is then marked as *failed* if the outage probability, P_{out}, on either or both the UL and DL transmission associated to the same sensor/actuator pair is larger than $P_{\text{out},T}$.

We evaluate the performance of the WIRT network in terms of *probability of loop failure* (PLF). Denoting the sets of sensor-to-controller and controller-to-actuator links with outage probability greater than $P_{\text{out},T}$ as $\mathcal{S}_{\text{UL}}$ and $\mathcal{S}_{\text{DL}}$, respectively, the PLF can be calculated as

$$\text{PLF} = \frac{|\mathcal{S}_{\text{UL}} \cup \mathcal{S}_{\text{DL}}|}{N_{\text{total}}}, \quad (2)$$

where $|\cdot|$ denotes the cardinality of the associated set, $\cup$ is the union operator, and N_{total} is the total number of communication loops in the scenario of interest.

While the outage probability, P_{out} is a device-level link performance indicator measuring the probability that packets transmitted from a given device will be lost in transit, the PLF reflects the capability of the network to deliver the expected service level at any location, and is therefore a measure of the overall spatial service availability.

In the following, we present SINR and the outage probability models used for our evaluation.

1) SINR MODEL
Let us assume a block-fading model where the channel bandwidth used at each TU is divided in L blocks, each experiencing uncorrelated fading.

The DL SINR of the nth actuator in subnetwork m on the ℓth block can be written as

$$
\Gamma_{nm,\ell}^{\mathrm{DL}}
$$
$$
= \frac{\gamma_{nm,\ell} P_{nm}}{\sum\limits_{\substack{k=1 \\ k \neq m}}^{M} \beta_{nmk} \gamma_{nmk,\ell} P_{nmk} + \sum\limits_{\substack{k=1 \\ k \neq m}}^{M} \sum\limits_{j=1}^{N} \beta_{nmjk} \gamma_{nmjk,\ell} P_{nmjk} + \sigma^2},
$$
(3)

where

- $\gamma_{nm,\ell}$ and P_{nm} denote the power gain of the small scale fading component and average power for the desired link between the nth actuator and the mth controller;
- $\gamma_{nmk,\ell}$ ($\gamma_{nmjk,\ell}$), P_{nmk} (P_{nmjk}), β_{nmk} (β_{nmjk}) are the small scale power gain, large scale interference power, and synchronization mismatch factor from the kth controller (jth device in the kth cell) to the nth device in cell m. The synchronization mismatch factor denotes the fraction of interference coming from a controller or a sensor in the neighbor subnetwork.
- σ^2 is the received thermal noise power per block.

The large scale desired or interfering signal power is calculated as (subscript indexes suppressed for simplicity) $P = 10^{P_{\mathrm{rx}}[\mathrm{dBm}]/10}$, where

$$
P_{\mathrm{rx}} [\mathrm{dBm}] = P_{\mathrm{tx}} [\mathrm{dBm}] - \mathrm{LS} [\mathrm{dB}],
$$

with P_{tx} denoting the transmit power and LS, the large scale propagation effect, embedding the effect of path-loss and shadowing. We consider the close-in (CI) free space reference distance models [56] which has been used extensively for analyzing path-loss and shadow fading in industrial channel measurements (see e.g., [57], [58]). Thus,

$$
\mathrm{LS} [\mathrm{dB}] = 20 \log_{10} \left(\frac{4 \pi f d_0}{c} \right) + 10 \varepsilon \log_{10} \left(\frac{d}{d_0} \right) + X_s [\mathrm{dB}],
$$
(4)

where $c \sim 3 \cdot 10^8$ m/s is the speed of light, d is the distance between the transmitter and receiver, $d_0 = 1$ m is the reference distance, ε denotes the path-loss exponent, f is the center frequency and X_s denotes the shadow fading component (in dB) which is modelled as a zero mean normal random variable with standard deviation σ_s.

The thermal noise power per block is instead calculated as

$$
\sigma^2 = 10^{(-174 + \mathrm{NF}[dB] + 10 \log_{10}(\mathrm{w}))/10}.
$$
(5)

Here, NF and w denote the receiver noise figure and bandwidth per block, respectively.

Let us consider the interference terms in the denominator of (3) which are summation of the large scale interference power weighted by the random small scale power gain, γ. In the limit of large number of subnetworks, M, γ in the sum can be replaced by the mean $\bar{\gamma}$, i.e., $\sum\limits_{\substack{m=1 \\ M \to \infty}}^{M} \gamma_m P_m \simeq \bar{\gamma} \sum\limits_{m=1}^{M} P_m$.

Applying this approximation to the denominator of (3) and substituting $\bar{\gamma} = 1$ yields

$$
\Gamma_{nm,\ell}^{\mathrm{DL}} = \frac{\gamma_{nm,\ell} P_{nm}}{\sum\limits_{\substack{k=1 \\ k \neq m}}^{M} \beta_{nmk} P_{nmk} + \sum\limits_{\substack{k=1 \\ k \neq m}}^{M} \sum\limits_{j=1}^{N} \beta_{nmjk} P_{nmjk} + \sigma^2}.
$$
(6)

The average DL SINR per channel is obtained by taking expectation of (6) over all fading blocks. Thus,

$$
\Gamma_{nm}^{\mathrm{DL}} = \frac{P_{nm}}{\sum\limits_{\substack{k=1 \\ k \neq m}}^{M} \beta_{nmk} P_{nmk} + \sum\limits_{\substack{k=1 \\ k \neq m}}^{M} \sum\limits_{j=1}^{N} \beta_{nmjk} P_{nmjk} + \sigma^2}.
$$
(7)

Following a similar procedure, the average UL SINR per channel is obtained as

$$
\Gamma_{nm}^{\mathrm{UL}} = \frac{P_{mn}}{\sum\limits_{\substack{k=1 \\ k \neq m}}^{M} \sum\limits_{j=1}^{N} \beta_{mnjk} P_{mnjk} + \sum\limits_{\substack{k=1 \\ k \neq m}}^{M} \beta_{mnk} P_{mnk} + \sigma^2}.
$$
(8)

For convenience, we will henceforth drop the device and subnetwork subscript indexing.

2) OUTAGE PROBABILITY

Let us assume that a packet of B bits is mapped at each TU over the entire channel bandwidth $W = L\mathrm{w}$, comprising of n OFDM symbols with d data subcarriers each; the transmission rate R is then given by

$$
R = \frac{B}{nd}.
$$
(9)

We further assume that capacity-achieving codes are adopted. In case of N_{rx} uncorrelated receive antennas and multiple independent packet repetitions, energy of the multiple transmissions can be coherently combined even in case of previous failures. This process is known in cellular communication as chase combining [59]. Eliminating the link indexing in (7) or (8), the outage probability after v repetitions can be expressed as

$$
P_{\mathrm{out},v} = \mathrm{Prob} \left[\frac{1}{L} \sum\limits_{\ell=1}^{L} \log_2 \left(1 + \sum\limits_{z=1}^{N_{\mathrm{rx}}} \sum\limits_{p=1}^{v} \gamma_{\ell,z,p} \Gamma_p \right) < R \right],
$$
(10)

where Γ_p denotes the average SINR on the pth channel and $\gamma_{\ell,z,p}$ is the small scale power for the zth receive antenna on the ℓth fading block of the pth channel. Consider the term $\sum_{p=1}^{v} \gamma_{\ell,z,p} \Gamma_p$ in (10) which is a weighted sum of random variables, $\{\gamma_{\ell,z,p}\}_{p=1}^{v}$ with same distribution and parameter(s). It is straightforward to show that $\sum_{p=1}^{v} \gamma_{\ell,z,p} \Gamma_p$ has the same distribution as $\gamma_{\ell,z} \sum_{p=1}^{v} \Gamma_p$, i.e., $\sum_{p=1}^{v} \gamma_{\ell,z,p} \Gamma_p \overset{d}{=} \gamma_{\ell,z} \sum_{p=1}^{v} \Gamma_p$, where $\gamma_{\ell,z}$ has the same distribution as $\{\gamma_{\ell,z,p}\}_{p=1}^{v}$. Thus, (10) can analogously be written as

$$
P_{\mathrm{out},v} = \mathrm{Prob} \left[\frac{1}{L} \sum\limits_{\ell=1}^{L} \log_2 \left(1 + \sum\limits_{z=1}^{N_{\mathrm{rx}}} \gamma_{\ell,z} \sum\limits_{p=1}^{v} \Gamma_p \right) < R \right].
$$
(11)

The outage probability over all N_{rep} repetitions is then computed as

$$P_{\text{out}} = \prod_{v=1}^{N_{\text{rep}}} P_{\text{out},v}. \tag{12}$$

Given the transmission parameters: L, N_{rep}, N_{rx}, the average SINR, $\{\Gamma_p\}_{p=1}^{N_{\text{rep}}}$, and the transmission rate, R, the probability of outage can be estimated using (11) and (12) via Monte Carlo generation of the channel small scale gain, $\gamma_{\ell,z}$, with predefined fading distribution.

Note that the outage probability in (10) is calculated assuming capacity-achieving codes. It is well-known that commonly used code can approach capacity only for large code-blocks [60], which may not be the case of the control and command packets used in WIRT. Nonetheless, using capacity-achieving codes prevents us from making specific assumptions on the channel coding scheme to be used, which is left as future design choice for WIRT. Moreover, the recent theory of limited block-length coding reveals marginal gap with Shannon capacities even for code-blocks of a few hundreds bits [61]. Also, (10) assumes ideal channel knowledge at the receiver, while in practice channel response for coherent detection is estimated from the reference signals and can deviate from the ideal one.

Given such idealistic assumptions, the simulation results presented in this article can be seen as optimistic bounds, and a performance penalty is expected in case realistic models for channel coding and channel estimation are in place.

B. SIMULATION PROCEDURE

Based on the scenario described in Section V-A, we evaluate the expected performance of WIRT networks via Monte Carlo simulations over a sufficiently large number of deployment snapshots. The number of snapshots is selected such that the PLF limit of 10^{-6} can be estimated with high statistical confidence. By applying the normal approximation of the Binomial proportion confidence interval, the required number of independent samples (i.e., the total number of devices over all snapshots) can be expressed as $N_{\text{samp}} = z_{\alpha/2}^2 (1-\hat{p})/(\epsilon \hat{p})$ [62]; where $\hat{p}$ denotes estimate of the proportion corresponding in our case to the 10^{-6} target PLF, ϵ is the error margin, $z_{\alpha/2}$ is the $100(1-\alpha/2)$-th percentile of the standard normal distribution and α is the confidence level. For each simulation the number of samples is set to $N_{\text{samp}} = 1.536 \times 10^8$ translating to a confidence level of about 95% within a 16% interval. The simulation involves the following steps:

1) **Deployment generation:** Within each snap-shot, the layout is created by placing controllers within the deployment area and uniformly distributing devices within a circular cell with radius, r_{cell}, centered at the position of each controller. As mentioned above, we assume in this study that the sensors and controllers are co-located.

2) **Channel Assignment:** Given a predefined frame structure, devices in each subnetwork are allocated orthogonal channels per each TUs, including repetitions.

The channel hopping pattern is different at each subnetwork. This is meant to randomize the interference and avoid a certain device to be persistently interfered by the same devices when transmitting its packet repetitions over multiple channels.

3) **Power and SINR computation:** The received signal power and interference power level are calculated using (4) by considering the distances for desired and interfering links in the deployment. The UL and DL SINR for each loop are then calculated using (7) and (8), respectively.

4) **Outage Probability mapping:** The average DL and UL SINR at each link are mapped to an outage probability value using (10). For practical purposes, the theoretical outage probability curves are calculated beforehand over a range of SINRs.

5) **PLF calculation:** As stated above, a loop is defined unsuccessful if either or both the associated UL and DL outage probabilities are higher than $P_{\text{out},T}$. The PLF is then calculated as ratio of the number of failed loops over multiple snapshots to the total number of loops.

Note that the outage probability calculation is based on the assumption that the average SINR is constant for each link. This represents the case of a fully static scenario at a given simulation snapshot. However, the average link SINR is recalculated for successive snapshots. In scenarios where the subnetworks are moving, temporal evolution of the SINR and other associated metrics must be modelled using appropriate correlated channel models.

In spite of these limitations, we believe the presented methodology can offer valuable insights on the expected performance trends in dense WIRT networks. Further analysis considering the effect of mobility, dynamic channel allocation, effect of channel imperfections and realistic codes is left for future work.
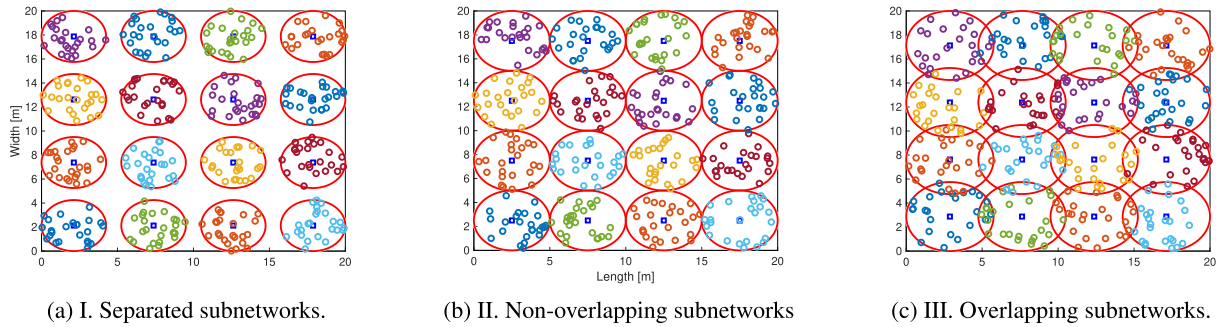
VI. PERFORMANCE EVALUATION

We are aiming at evaluating the required bandwidth for supporting a predefined PLF target in a dense WIRT network. If the latency, reliability and availability targets are fulfilled in such deployments, we can also conclude that a WIRT network would be able to operate successfully in less dense scenarios.

We define 8 different configurations where the channel bandwidth size ranges from 40 MHz to 320 MHz. A total of $N_{\text{ch}} = 12$ channels is assumed, leading to overall bandwidth sizes ranging from 480 MHz to 3.84 GHz. The general parameters associated to the configurations are presented in Table 2. A packet size of 50 bytes is considered for both sensor-to-controller and controller-to-actuator links. This is consistent with 3GPP assumptions for URLLC studies in industrial scenarios [51]. Note that a given packet size leads to different transmission rates depending on the bandwidth according to (9), and therefore to different outage probabilities. A 90 μs frame is assumed, consisting of 20 TUs per suframe. By setting a subcarrier spacing of 480 kHz, a TU can be mapped over a single OFDM symbol. For all bandwidth

TABLE 2. Considered per channel bandwidth sizes and associated parameters for performance evaluation.

Parameter	Configurations							
	40 MHz	80 MHz	120 MHz	160 MHz	200 MHz	240 MHz	280 MHz	320 MHz
Packet size [bytes]	50	50	50	50	50	50	50	50
Number of channels	12	12	12	12	12	12	12	12
Total bandwidth [MHz]	480	760	1440	1920	2400	2880	3360	3940
Number of TUs per subframe	20	20	20	20	20	20	20	20
Subcarrier spacing [kHz]	480	480	480	480	480	480	480	480
Number of subcarriers per channel	83	166	250	333	416	500	583	666
Number of data subcarriers per channel	66	133	200	266	333	400	466	533
Number of OFDM symbols per TU	1	1	1	1	1	1	1	1
Max number of control loops	48	48	48	48	48	48	48	48
Transmission rate, R [bits/s/Hz]	6.06	3.01	2.00	1.50	1.20	1.00	0.85	0.75
Uncorrelated fading blocks per channel	2	4	6	8	10	12	14	16
Number of receive antennas	[2,4]	[2,4]	[2,4]	[2,4]	[2,4]	[2,4]	[2,4]	[2,4]

(a) I. Separated subnetworks. (b) II. Non-overlapping subnetworks (c) III. Overlapping subnetworks.

FIGURE 4. Example of considered deployments. The inter-distance, d_c is fixed at 5 m. The subnetwork radius are $r_{cell} = 2.0$ m, $r_{cell} = 2.5$ m and $r_{cell} = 3.0$ m for deployments I, II and III, respectively.

configurations, it is assumed that only 80% of the subcarriers are dedicated to data, while reference sequences for coherent detection are mapped over the remaining subcarriers. We assume for simplicity that both controller and devices are equipped with a single transmit antenna and a maximum of 4 receive antennas; the small form factor of sensors and actuators may indeed prevent the usage of a larger number of antennas. Note that we refer here to up to 4 radio-frequency chains, which might not be supported by low cost devices. One can envision different device categories for WIRT, e.g., 2 antennas low class devices, and 4 antennas for high class devices.

The general parameters of the deployments considered in the simulations are reported in Table 3 along with radio propagation parameters. Each deployment consists of $M = 16$ subnetworks with fixed controller positions with inter-subnetwork distance, $d_c = 5$ m, in a 20 m × 20 m rectangular area. To investigate the effect of deployment choices on achievable performance, we consider the 3 scenarios in Figure 4 with different service - to - cell area ratio, calculated as $\varepsilon = 2 \cdot r_{cell}/d_c$:

 I. Separated subnetworks with $\varepsilon = 0.8$.
 II. Non-overlapping subnetworks with $\varepsilon = 1.0$.
 III. Partially overlapping subnetworks with $\varepsilon = 1.2$.

We will refer to these deployments as I (separated), II (non-overlapping) and III (overlapping) throughout this article. Note that such scenarios reflect a density

TABLE 3. Simulation parameters.

Parameter	Value
Deployment Parameters	
Area	20 m × 20 m
Device density, ρ	[0.5 1.0 2.0]/m²
Subnetwork density	40000/km²
Inter-subnetwork distance, d_c	5 m
Number of controllers/subnetworks, N	16
Number of devices per subnetwork, M	[12 24 48]
Propagation and System Parameters	
PL exponent, ε	2.7
Shadowing standard deviation, σ_s	3
Noise Figure (NF)	10dB
Power density per channel	-10 dBm
Lowest Frequency	6 GHz
Number of repetitions, N_{rep}	1 - 4

of 40000 subnetworks/km². Assuming a maximum of 4 packet repetitions, the maximum number of sensor-actuator pairs per subnetwork supported by the frame configuration presented above is obtained from (1) to be 48. In our deployment, this corresponds to a device density $\rho = 2.0$ devices/m². Lower number of devices per subnetwork (12 and 24, corresponding to densities $\rho = 0.5$ devices/m² and $\rho = 1.0$ devices/m², respectively), are also considered.

The radio propagation parameters are set based on recent measurements in industrial environments. In [56], ε and σ_s

were reported to be in the range 1.2 to 2.94 and 1.59 dB to 2.4 dB, respectively. A recent industrial channel measurements study [63] also reported a range of values from 0.98 to 3.0 and 2.53 dB to 5.23 dB for ε and σ_s, respectively. Similar parameter values were also reported in [57], [58]. Since the large scale fading parameters are selected from industrial measurements, obtained performance results is expected to be more accurate for industrial control applications than for other use cases. For instance, WIRT subnetworks in intra-vehicle scenario may suffer higher shadowing on the desired path due to blockage from tightly packed parts. These subnetworks will also benefit from increased isolation due to metallic shielding and hence, from weaker interference power. We therefore, expect the obtained results to offer reasonable insights for all use cases and leave further scenario-specific evaluations to future work.

We assume that the small scale fading follows a Rayleigh distribution. The Rayleigh fading has been identified as a suitable model in industrial scenarios given the massive presence of metallic reflectors and scatterers that contribute to the received power [64]. The small scale fading power coefficients, γ, in (10) follow then an exponential distribution. The number of fading blocks is calculated assuming 20 MHz bandwidth per block.

For all configurations, we assume contiguous bandwidth allocations with 6 GHz being the lower frequency. In the case of the 40 MHz configuration, the overall bandwidth allocation would then be 6 GHz - 6.48 GHz, while for the 320 MHz per channel configuration it is 6 GHz - 9.84 GHz. The large scale pathloss effects in (4) take into account the variations in carrier frequency across the operational bandwidth.

A. RESULTS

We now present a selection of relevant results aiming at illustrating the WIRT performance with the different parameter combinations in Table 2. Fig. 5 shows the outage probability for all configurations computed using (10) and a single channel ($v = 1$). As expected, increasing the bandwidth and the receive diversity order translates to a major reduction of the required SINR for coping with a certain outage probability target. In particular, a large bandwidth allows to benefit from frequency diversity gain and coding gain, given the low coding rate. The major benefits of doubling the number of receive antennas are due to the combination of diversity and array gains. With 4 receive antennas and a channel bandwidth $\geq$ 200 MHz, an outage probability below 10^{-6} can be obtained even at SINRs lower than 0 dB. Also, curves become very steep for large bands and a high degree of diversity; a minor variation of SINR can then lead to a dramatic increase/decrease of the outage probability. The theoretical outage curves in Fig. 5 are used as reference for mapping computed SINR to outage probability in subsequent results.

The next results show the overall network performance, and are obtained with transmit power per channel, P_{ch}, of -10 dBm. For the sensors, this corresponds to the
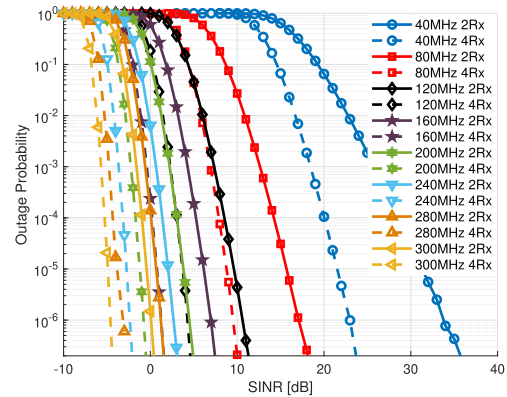

FIGURE 5. Outage probability curves for different per channel bandwidth. 2Rx and 4Rx denote 2 and 4 receive antennas, respectively.
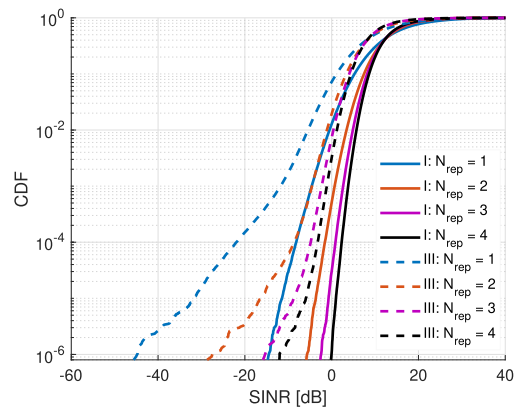

FIGURE 6. Distribution of combined SINR for different number of repetitions with device density of 1.0/m², 4 receive antennas and 12 frequency channels. The SINR values are obtained by summing per channel values over all repetitions.

instantaneous transmit power since they are operating over a single channel at a time. For the controller, the overall transmit power could be up to $P = P_{ch} + 10 \log_{10} N_{ch} \approx$ 0.8 dBm in cases where all $N_{ch} = 12$ channels are occupied instantaneously. Our preliminary simulation tests have indeed shown that this power level leads to reasonable SINR values throughout the entire network and that no benefits are visible when operating with a higher power. This is due to the short transmission range and the interference-limited nature of the deployment scenarios.

In Fig. 6, we show the cumulative distribution function (CDF) of the combined SINR over different number of repetitions for deployments I and III with device density of 1.0/m². As expected, increasing the number of repetitions results in an increase in SINR thanks to the combining of the useful energy. However, the SINR improvement diminishes as the total number of repetitions increases, with a marginal gain when moving from 3 to 4 repetitions.

The figure also shows that cell overlap significantly degrades SINR. For example, for a single transmission ($N_{rep} = 1$), there is approximately a 30 dB margin between the deployments I and III in the tail of the CDF curves
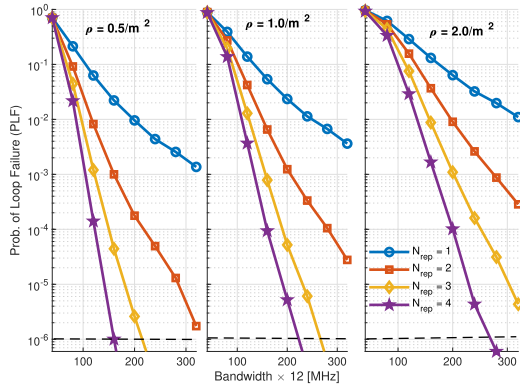
FIGURE 7. Effect of bandwidth and transmission repetitions on loop failure probability with deployment II, 4 receive antennas and 12 frequency channels.

FIGURE 8. Effects of cell overlap and density on loop failure probability with 4 receive antennas.

FIGURE 9. Effects of number of receive antennas on loop failure probability with deployment II. The number of receive antennas and device density combinations with bars at the $\leq 10^{-6}$ mark indicate PLF lower than or equal to 10^{-6}.

in Fig. 6. The relative benefits of repetitions are instead larger for deployment III, reducing the gap at the tail of the CDF curves to ∼12 dB for the case of 4 repetitions. Observe that repetitions also reduce the spread of the SINR curves. A plausible explanation for this is that the large frequency diversity and energy combining diminishes significantly the small scale fading effects resulting the instantaneous SINRs becoming nearly equal to the average SINRs of the links. Let us now quantify the achievable performance in terms of PLF. Except where stated otherwise, we consider an outage probability target of $P_{\text{out,T}} = 10^{-6}$. We show the effect of bandwidth and repetitions on PLF for deployment II in Fig. 7. Similar to the outage probability, we set a target of $\leq 10^{-6}$ on the PLF. Note that lower values of PLF can be simulated but requires much more processing power and simulation efforts. As expected, the PLF decreases with increasing bandwidth and/or number of repetitions. In case of single transmission ($N_{rep} = 1$), a PLF lower than 10^{-3} cannot be achieved even for a low device density for any of the configurations. For $\rho = 0.5/\text{m}^2$, a channel bandwidth of 160 MHz suffices for achieving the PLF target of 10^{-6} with 4 repetitions, while for high device density a channel bandwidth larger than 300 MHz might be needed.

In Fig. 8, we illustrate the impact of deployment option as well as device density on the PLF, considering 4 receive antennas and 4 repetitions. As expected, due to the weaker interfering links, deployment I with separated subnetworks yields the lowest PLF at all device densities. A PLF value of $\leq 10^{-6}$ is achieved for this deployment with per channel (total bandwidth) between ≥ 160 MHz (≥ 1920 MHz) and ≥ 200 MHz (≥ 2400 MHz) for device density between $0.5/\text{m}^2$ and $2.0/\text{m}^2$. For deployment II, the $\leq 10^{-6}$ PLF target is achieved at per channel bandwidth of ∼ 160 MHz and ∼ 200 MHz with device density $\rho = 0.5/\text{m}^2$ and $\rho = 1.0/\text{m}^2$, respectively. The scenario in deployment III requires significantly higher bandwidth to achieve the PLF target at all device density values. This is expected considering the poor SINR performance of the deployment in Fig. 6.

We show the effect of number of receive antennas in Fig. 9 where we plot the PLF for deployment II with 2 or 4 receive
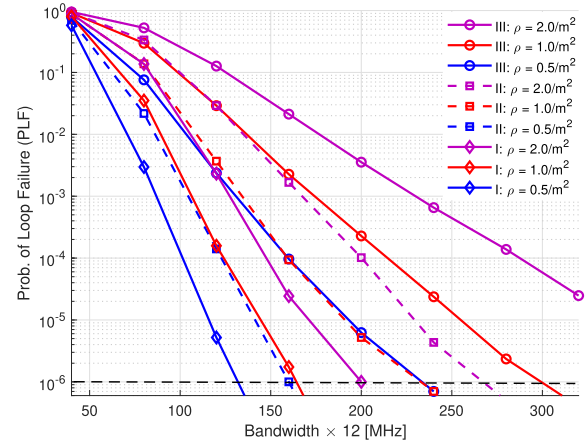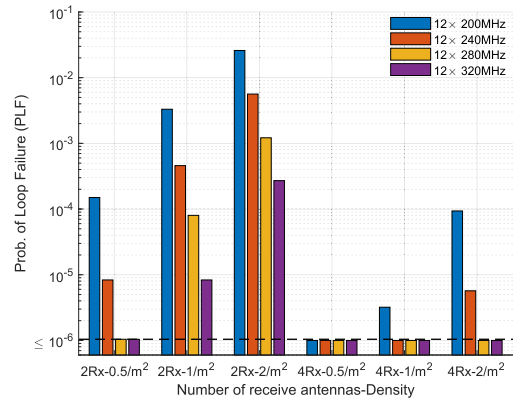
antennas and different bandwidth sizes. As a consequence of the spatial diversity gain, increase in number of antennas from 2 to 4 results in significant decrease in PLF. For the $\rho = 0.5/\text{m}^2$ case with channel bandwidth greater than or equal to 280 MHz, the target is achieved with 2 receive antennas. All other configurations require 4 receive antennas to meet the stringent limit on loop failure.

We present a summary of the required bandwidth configurations to achieve a $\leq 10^{-6}$ outage probability and a PLF $\leq 10^{-6}$ in Fig. 10. The case of deployment with overlapping subnetworks and high device density requires larger bandwidth than the maximum of 3840 MHz in our simulations. The deployment with separated subnetworks and a low device density can instead achieve the target with a 1920 MHz bandwidth. Observe that the impact of the device density on the required bandwidth is more pronounced in deployments II and III, due to the higher interference levels. It should also be noted that the bandwidth values are a consequence of the chosen configurations and assumptions for our simulations, with a coarse 40 MHz spacing between per channel bandwidth
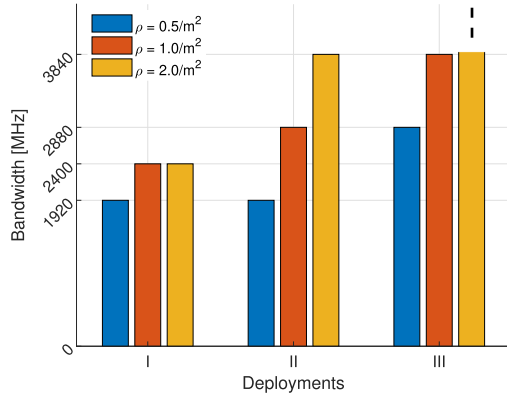
FIGURE 10. Approximate bandwidth requirement to support control loops with ≤ 0.1 ms latency, $\leq 10^{-6}$ reliability and below $\leq 10^{-6}$ probability of failure with 4 receive antennas. The dashed line indicate that the bandwidth required for deployment III with a 2/m^2 device density is above the limit in our simulations.
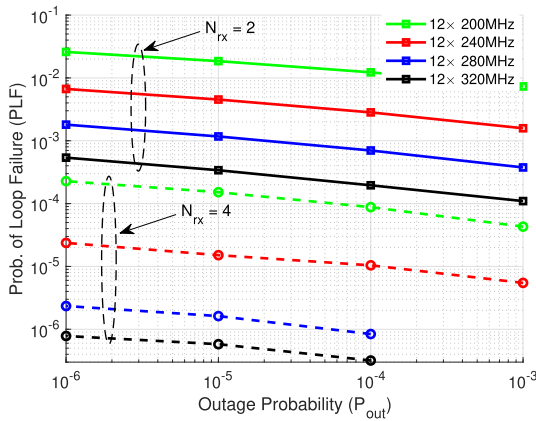

FIGURE 11. Loop failure probability versus outage probability for deployment III with device density 1/m^2 and 4 repetitions.

(and equivalently 480 MHz spacing between total bandwidth options).

The analysis so far considered a target of $\leq 10^{-6}$ on both outage probability and PLF. Fig. 11 shows instead the dependency of PLF from the outage probability target, considering deployment III with $\rho = 1/m^2$. Interestingly, PLF shows a weak dependency from the outage probability target; relaxing the outage probability target from 10^{-6} to 10^{-3} only reduces the PLF by a factor of $\sim \times 3\text{-}5$. This is a consequence of the steep nature of the outage-SINR curves in Fig. 5, i.e., for a configuration with a sufficiently large number of repetitions, a large difference in outage probability can be obtained with a very minor SINR improvement. The support of control loops that can tolerate a more relaxed outage probability, does not translate then to a major improvement in terms of spatial availability of the service.

B. DISCUSSION

Results presented above have shown that a multi-GHz spectrum might be needed to wirelessly support control loops shorter than 0.1 ms with a large spatial availability in a dense

WIRT network. Also, results have highlighted the major benefits of packet repetitions and multi-antenna receivers.

As mentioned above, performance results can be subject to a further penalty if more realistic models on channel codes and non-ideal channel estimation is to be considered. Nonetheless, the relative trends and performance gaps among the sensitive parameters (number of repetitions, receive antennas, channel sizes) are expected not to be affected.

Also, the analysis assumed a fixed allocation of the channels per link. In dynamic channel allocation schemes, subnetworks should be able to sense the interference levels on the channels allocated to each device, and eventually modify their hopping pattern while ensuring orthogonality to the other served devices. Such solutions are expected to be reduce the overall mutual interference levels, potentially translating to a reduction of the required spectrum. Approaches based on games theory [65]–[69], genetic algorithms [70], or neural networks [71] are to be explored. Also, power control [72] and link adaptation [73] are expected to have benefits in terms of spectrum reduction thanks to their capabilities of reducing resource expenditure and therefore interference footprint in the network.

The large bandwidth requirements poses obvious challenges for the support of such services in the centimeter-wave spectrum. As mentioned in Section III, centimeter-wave spectrum is indeed largely populated and even future 5G bands in the 6 GHz spectrum do not suffice for accommodating WIRT services.

On the other side, the favorable propagation conditions in this spectrum region and the short range allow operation with very low power (e.g., -10 dBm as considered in the above analysis). This suggests the possibility of operating WIRT as an underlay network over bands potentially occupied by other systems. In spite of its apparent saturation, centimeter-wave is also known to be largely underutilized on a spatial and temporal basis [74], offering a tremendous opportunity for WIRT.

The operational principle can be analogous to Ultra Wideband (UWB) technology, which provides unlicensed access to a broad spectrum [75], [76]. FCC and the ITU define UWB as an antenna transmission for which the emitted signal bandwidth exceeds the lesser of 500 MHz or 20% of the arithmetic center frequency. In Europe, UWB signals must have instead a minimum bandwidth of 50 MHz. For indoor applications, the FCC imposes a maximum mean Equivalent Isotropically Radiated Power (EIRP) of -41.3 dBm/MHz and a peak EIRP of 0 dBm/50 MHz over the 3.1 GHz-10.6 GHz range [77], while ECC adopts the same limitations for generic applications but over a reduced range (6-8.5 GHz) [78]. Operating over different frequency regions imposes the application of further mitigation techniques such as Detect and Avoid (DAA). The low power spectral density allows UWB transmissions to operate as underlay links that do not harm other radio systems active in the same spectrum. Also, coexisting radio systems are seen as narrowband interferers by UWB links, and therefore are expected to have a minor impact on

their performance. UWB is an optional physical layer in the IEEE 802.15.4 standard for Low-Rate Wireless PANs (LR-WPANs) [79], and is currently used mainly for localization applications [80]. The low transmit power makes UWB a suitable technology for short range transmission, and the large accessible bandwidth makes it also attractive for WIRT. Also, underlay UWB systems operate in unlicensed mode, but without the obligation of using a CCA mechanism for channel access.

In our simulations, each sensor is transmitting on a given channel every $2N_{TU} = 40$ TUs resulting in a duty cycle of $1/40$, i.e., 2.5%. Thus, the UWB power spectral limit for transmission over a 320 MHz channel would lead to a maximum instantaneous transmit power of ≈ -0.2dBm,[1] which is significantly larger than the -10 dBm value used; the presented study is therefore within the accepted limit of UWB regulations at least for the UL. In the DL, the duty cycle is up to 50%, and the respective power density per channel will be lower, i.e., in the order of ≈ -19 dBm. Potential new regulations are then needed in order to run WIRT as an underlay system in the below 10 GHz spectrum. Also, intelligent mechanisms to deal with external interference might be needed in order to preserve the required communication quality.

VII. CONCLUSION

We have presented the design of a wireless isochronous real time (WIRT) system for closed loop control applications. The system consists of short range low power subnetworks designed for services with very stringent reliability ($\leq 10^{-6}$) and extremely short cycles (≤ 0.1 ms) such as industrial sensor-actuator level control, or intra-vehicle communication for engine and suspension control. Design aspects including frame structure and transmission techniques have been extensively discussed, with focus on the centimeter-wave spectrum region. Performance of the system is evaluated via a semi-analytical procedure considering a dense deployment with device densities up to $2/m^2$. Results show that a multi-GHz spectrum is required to achieve large spatial service availability. On the other side, short range transmission and favorable propagation conditions in the centimeter-wave spectrum region enable the possibility of running WIRT as an underlay system over spectra where other systems can potentially be active, similarly to UWB technology. Investigation of other enhancements such as link adaptation, dynamic channel allocation, interference management and multiplexing of the unidirectional data plane with bidirectional control plane is part of our ongoing research.

APPENDIX
PROOF OF (1)

Let us define as a group, the set of TUs where concurrently interleaved devices are performing their transmissions

---

[1] The power density per channel, P is related to bandwidth (W [MHz]) and duty cycle (DC [%]) via $P = -41.3 + 10\log_{10}W - 10\log_{10}\frac{DC}{100}$.

(including repetitions). For example, in Figure 3, a group corresponds to the set of the first 6 TUs, where devices a,b,c,d,e,f and g,h,i,j,k,l are transmitting. Since each group has a size equal to $2N_{\text{rep}}$, the number of supported groups in a subframe is given by $N_{gr} = \left\lfloor \frac{N_{TU}}{2N_{\text{rep}}} \right\rfloor$, and the total number of loops supported in the N_{gr} blocks is

$$N_d = \left\lfloor \frac{N_{TU}}{2N_{\text{rep}}} \right\rfloor 2N_{\text{ch}}. \tag{13}$$

The remaining TUs in the subframe are then $N_{TU} - \left\lfloor \frac{N_{TU}}{2N_{\text{rep}}} \right\rfloor 2N_{\text{rep}}$ which can accommodate another set of N_{ch} devices if their number is at least equal to $2N_{\text{rep}} - 1$. The number N_{extra} of additional loops that can then be supported in the frame is equal to

$$N_{\text{extra}} = \left\lfloor \frac{N_{TU} - \left\lfloor \frac{N_{TU}}{2N_{\text{rep}}} \right\rfloor 2N_{\text{rep}}}{2N_{\text{rep}} - 1} \right\rfloor N_{\text{ch}} \tag{14}$$

By summing (13) and (14), we obtain (1).

REFERENCES

[1] B. Chen, J. Wan, L. Shu, P. Li, M. Mukherjee, and B. Yin, "Smart factory of industry 4.0: Key technologies, application case, and challenges," *IEEE Access*, vol. 6, pp. 6505–6519, 2018.
[2] R. Y. Zhong, X. Xu, E. Klotz, and S. T. Newman, "Intelligent manufacturing in the context of industry 4.0: A review," *Engineering*, vol. 3, no. 5, pp. 616–630, Oct. 2017.
[3] D. Jansen and H. Buttner, "Real-time Ethernet: The EtherCAT solution," *Comput. Control Eng.*, vol. 15, no. 1, pp. 16–21, Feb. 2004.
[4] B. Galloway and G. P. Hancke, "Introduction to industrial control networks," *IEEE Commun. Surveys Tuts.*, vol. 15, no. 2, pp. 860–880, 2nd Quart., 2013.
[5] S. Simatic, "PROFINET system description," SIEMENS, Munich, Germany, Syst. Manual A5E00298288-04, 2008, vol. 6.
[6] L. Lo Bello and W. Steiner, "A perspective on IEEE time-sensitive networking for industrial communication and automation systems," *Proc. IEEE*, vol. 107, no. 6, pp. 1094–1120, Jun. 2019.
[7] A. Nasrallah, A. S. Thyagaturu, Z. Alharbi, C. Wang, X. Shao, M. Reisslein, and H. ElBakoury, "Ultra-low latency (ULL) networks: The IEEE TSN and IETF DetNet standards and related 5G ULL research," *IEEE Commun. Surveys Tuts.*, vol. 21, no. 1, pp. 88–145, 1st Quart., 2019.
[8] S. Tuohy, M. Glavin, C. Hughes, E. Jones, M. Trivedi, and L. Kilmartin, "Intra-vehicle networks: A review," *IEEE Trans. Intell. Transp. Syst.*, vol. 16, no. 2, pp. 534–545, Apr. 2015.
[9] *IEEE Standard for Low-Rate Wireless Networks*, IEEE Standard 802.15.4-2015, Dec. 2015.
[10] *IEEE Standard for Information Technology—Telecommunications and Information Exchange Between Systems Local and Metropolitan Area Networks—Specific Requirements—Part 11: Wireless LAN Medium Access Control (MAC) and Physical Layer (PHY) Specifications*, IEEE Standard 802.11-2016, Dec. 2016.
[11] J.-E. Frey, "WISA–wireless control in theory, practice and production," in *Proc. IEEE Int. Conf. Emerg. Technol. Factory Autom.*, Sep. 2008, p. 7.
[12] J. Song, S. Han, A. Mok, D. Chen, M. Lucas, M. Nixon, and W. Pratt, "WirelessHART: Applying wireless technology in real-time industrial process control," in *Proc. IEEE Real-Time Embedded Technol. Appl. Symp.*, Apr. 2008, pp. 377–386.
[13] *Wireless Systems for Industrial Automation: Process Control and Related Applications*, document ANSI/ISA-100.11 a-2009, 2009.
[14] W. Liang, X. Zhang, Y. Xiao, F. Wang, P. Zeng, and H. Yu, "Survey and experiments of WIA-PA specification of industrial wireless network," *Wireless Commun. Mobile Comput.*, vol. 11, no. 8, pp. 1197–1212, Aug. 2011.
[15] *Industrial Networks—Wireless Communication Network and Communication Profiles—WIA-FA*, Standard IEC 62948, International Electrotechnical Commission (IEC), 2017.

[16] Z. Pang, M. Luvisotto, and D. Dzung, "Wireless high-performance communications: The challenges and opportunities of a new target," *IEEE Ind. Electron. Mag.*, vol. 11, no. 3, pp. 20–25, Sep. 2017.

[17] H. Holma and A. Toskala, *LTE for UMTS: OFDMA and SC-FDMA Based Radio Access.* Hoboken, NJ, USA: Wiley, 2009.

[18] *Physical Layer Procedures for Data (Release 15)*, document 38.214 v15.1.0, 3GPP, Mar. 2018.

[19] *IMT Vision—Framework and Overall Objectives of the Future Development of IMT for 2020 and Beyond*, Standard Rec. ITU-R M.2083-0, International Telecommunication Union (ITU), Radiocommunication Study Groups, Sep. 2015.

[20] T. Jacobsen, R. Abreu, G. Berardinelli, K. Pedersen, P. Mogensen, I. Z. Kovacs, and T. K. Madsen, "System level analysis of uplink grant-free transmission for URLLC," in *Proc. IEEE Globecom Workshops (GC Wkshps)*, Dec. 2017, pp. 1–6.

[21] A. A. Esswie and K. I. Pedersen, "Multi-user preemptive scheduling for critical low latency communications in 5G networks," in *Proc. IEEE Symp. Comput. Commun. (ISCC)*, Jun. 2018, p. 00136–00141.

[22] C. Mannweiler, B. Gajic, P. Rost, R. S. Ganesan, C. Markwart, R. Halfmann, J. Gebert, and A. Wich, "Reliable and deterministic mobile communications for industry 4.0: Key challenges and solutions for the integration of the 3GPP 5G system with IEEE," in *Proc. Mobile Commun.-Technol. Appl.; 24. ITG-Symp.*, May 2019, pp. 1–6.

[23] S. Tuohy, M. Glavin, C. Hughes, E. Jones, M. Trivedi, and L. Kilmartin, "Intra-vehicle networks: A review," *IEEE Trans. Intell. Transp. Syst.*, vol. 16, no. 2, pp. 534–545, Apr. 2015.

[24] M. Latva-aho and K. Leppänen. (2019). *Key Drivers and Research Challenges for 6G Ubiquitous Wireless Intelligence.* [Online]. Available: http://urn.fi/urn:isbn:9789526223544

[25] M. Luvisotto, Z. Pang, and D. Dzung, "High-performance wireless networks for industrial control applications: New targets and feasibility," *Proc. IEEE*, vol. 107, no. 6, pp. 1074–1093, Jun. 2019.

[26] G. Berardinelli, N. H. Mahmood, I. Rodriguez, and P. Mogensen, "Beyond 5G wireless IRT for industry 4.0: Design principles and spectrum aspects," in *Proc. IEEE Globecom Workshops (GC Wkshps)*, Dec. 2018, pp. 1–6.

[27] G. Berardinelli, P. E. Mogensen, and R. O. Adeogun, "6G subnetworks for life-critical communication," in *Proc. 6G Wireless Summit*, Mar. 2020, pp. 1–5.

[28] D. Lopez-Perez, M. Ding, H. Claussen, and A. H. Jafari, "Towards 1 Gbps/UE in cellular systems: Understanding ultra-dense small cell deployments," *IEEE Commun. Surveys Tuts.*, vol. 17, no. 4, pp. 2078–2101, 1st Quart., 2015.

[29] *Service Requirements for the 5G System; Stage 1 (Release 17)*, document 22.261 v17.0.1, 3GPP, 2019.

[30] J. Guerrero-Ibáñez, S. Zeadally, and J. Contreras-Castillo, "Sensor technologies for intelligent transportation systems," *Sensors*, vol. 18, no. 4, p. 1212, Apr. 2018.

[31] M. Ding, D. Lopez-Perez, H. Claussen, and M. A. Kaafar, "On the fundamental characteristics of ultra-dense small cell networks," *IEEE Netw.*, vol. 32, no. 3, pp. 92–100, May 2018.

[32] T. S. Rappaport, S. Sun, R. Mayzus, H. Zhao, Y. Azar, K. Wang, G. N. Wong, J. K. Schulz, M. Samimi, and F. Gutierrez, "Millimeter wave mobile communications for 5G cellular: It will work!" *IEEE Access*, vol. 1, pp. 335–349, 2013.

[33] R. O. Adeogun and O. E. Falowo, "Performance analysis of two-tier multiantenna 5G heterogeneous wireless networks with dual band transmission," in *Proc. 24th Int. Conf. Telecommun. (ICT)*, May 2017, pp. 1–6.

[34] H. Elayan, O. Amin, R. M. Shubair, and M.-S. Alouini, "Terahertz communication: The opportunities of wireless technology beyond 5G," in *Proc. Int. Conf. Adv. Commun. Technol. Netw. (CommNet)*, Apr. 2018, pp. 1–5.

[35] *User Equipment (UE) Radio Transmission and Reception; Part 1: Range 1 Standalone (Release 16)*, document 38.101 v16.0.0, 3GPP, Jun. 2019.

[36] Y. Henri, "ITU world radiocommunication conference (WRC-15) allocates spectrum for future innovation," *Air Space Law*, vol. 41, no. 2, pp. 119–128, 2016.

[37] M. M. Sohul, M. Yao, T. Yang, and J. H. Reed, "Spectrum access system for the citizen broadband radio service," *IEEE Commun. Mag.*, vol. 53, no. 7, pp. 18–25, Jul. 2015.

[38] M. Matinmikko, M. Latva-aho, P. Ahokangas, S. Yrjölä, and T. Koivumäki, "Micro operators to boost local service delivery in 5G," *Wireless Pers. Commun.*, vol. 95, no. 1, pp. 69–82, Jul. 2017.

[39] M. Centenaro, L. Vangelista, A. Zanella, and M. Zorzi, "Long-range communications in unlicensed bands: The rising stars in the IoT and smart city scenarios," *IEEE Wireless Commun.*, vol. 23, no. 5, pp. 60–67, Oct. 2016.

[40] M. Lauridsen, F. Frederiksen, and I. Rodriguez, "Feasibility of deploying wireless Internet of Things in the unlicensed European 865–868 MHz band," in *Proc. IEEE Wireless Commun. Netw. Conf. (WCNC)*, Apr. 2019, pp. 1–5.

[41] G. Zhou, J. A. Stankovic, and S. H. Son, "Crowded spectrum in wireless sensor networks," in *Proc. IEEE EmNets*, vol. 6, 2006, pp. 1–6.

[42] *Revision of Part 15 of the Commission's Rules to Permit Unlicensed National Information Infrastructure (U-NII) Devices in the 5 GHz Band*, FCC, Washington, DC, USA, Feb. 2004.

[43] *5 GHz RLAN; Harmonised Standard Covering the Essential Requirements of Article 3.2 of Directive 2014/53/EU*, document EN 301 893 V2.1.1, ETSI, May 2017.

[44] G. Naik, J. Liu, and J.-M. Park, "Coexistence of wireless technologies in the 5 GHz bands: A survey of existing solutions and a roadmap for future research," *IEEE Commun. Surveys Tuts.*, vol. 20, no. 3, pp. 1777–1798, 3rd Quart., 2018.

[45] G. Staple and K. Werbach, "The end of spectrum scarcity [spectrum allocation and utilization]," *IEEE Spectr.*, vol. 41, no. 3, pp. 48–52, Mar. 2004.

[46] T. Jacobsen, "Radio resource management for uplink grant-free ultra-reliable low-latency communications," Ph.D. dissertation, Aalborg Univ., Aalborg, Denmark, 2019.

[47] H. K. Choi and W. Kim, "Frequency-hopped spread spectrum multiple-access communication with nonorthogonal BFSK signaling in a Rayleigh fading channel," in *Proc. Int. Conf. Universal Pers. Commun.*, vol. 2, Oct. 1996, pp. 638–641.

[48] P. C. Chan, E. Lo, R. Wang, E. S. Au, V. N. Lau, R. Cheng, W. Mow, R. Murch, and K. Letaief, "The evolution path of 4G networks: FDD or TDD?" *IEEE Commun. Mag.*, vol. 44, no. 12, pp. 42–50, Dec. 2006.

[49] E. Ayanoglu, M. Burgess, M. Pollack, and A. Zamanian, "Frequency division duplexing and time division duplexing for broadband wireless applications," Broadband Wireless Internet Forum, White Paper, 2001, vol. 1, pp. 1–52.

[50] D. Catania, M. G. Sarret, A. F. Cattoni, F. Frederiksen, G. Berardinelli, and P. Mogensen, "The potential of flexible UL/DL slot assignment in 5G systems," in *Proc. 80th IEEE Veh. Technol. Conf.*, Sep. 2014, pp. 1–6.

[51] *Study on Communication for Automation in Vertical Domains (Release16)*, document 22.804 v16.2.0, 2018.

[52] K. Stadius, T. Rapinoja, J. Kaukovuori, J. Ryynanen, and K. A. I. Halonen, "Multitone fast frequency-hopping synthesizer for UWB radio," *IEEE Trans. Microw. Theory Techn.*, vol. 55, no. 8, pp. 1633–1641, Aug. 2007.

[53] R. V. Nee and R. Prasad, *OFDM for Wireless Multimedia Communications.* Norwood, MA, USA: Artech House, 2000.

[54] S.-Y. Lien, S.-L. Shieh, Y. Huang, B. Su, Y.-L. Hsu, and H.-Y. Wei, "5G new radio: Waveform, frame structure, multiple access, and initial access," *IEEE Commun. Mag.*, vol. 55, no. 6, pp. 64–71, Jun. 2017.

[55] F. Schaich and T. Wild, "Subcarrier spacing–a neglected degree of freedom?" in *Proc. IEEE 16th Int. Workshop Signal Process. Adv. Wireless Commun. (SPAWC)*, Jun. 2015, pp. 56–60.

[56] M. Düngen, T. Hansen, R. Croonenbroeck, R. Kays, B. Holfeld, D. Wieruch, P. W. Berenguer, V. Jungnickel, D. Block, U. Meier, and H. Schulze, "Channel measurement campaigns for wireless industrial automation," *at-Automatisierungstechnik*, vol. 67, no. 1, pp. 7–28, Jan. 2019.

[57] D. A. Wassie, I. Rodriguez, G. Berardinelli, F. M. L. Tavares, T. B. Sorensen, and P. Mogensen, "Radio propagation analysis of industrial scenarios within the context of ultra-reliable communication," in *Proc. IEEE 87th Veh. Technol. Conf. (VTC Spring)*, Jun. 2018, pp. 1–6.

[58] J. Karedal, S. Wyne, P. Almers, F. Tufvesson, and A. Molisch, "A measurement-based statistical model for industrial ultra-wideband channels," *IEEE Trans. Wireless Commun.*, vol. 6, no. 8, pp. 3028–3037, Aug. 2007.

[59] D. Chase, "A combined coding and modulation approach for communication over dispersive channels," *IEEE Trans. Commun.*, vol. 21, no. 3, pp. 159–174, Mar. 1973.

[60] S. Dolinar, D. Divsalar, and F. Pollara, "Code performance as a function of block size," Telecommun. Mission Oper. Prog. Rep., NASA, Washington, DC, USA, TMO Prog. Rep. 42-133, 1998.

[61] G. Durisi, T. Koch, and P. Popovski, "Toward massive, ultrareliable, and low-latency wireless communication with short packets," *Proc. IEEE*, vol. 104, no. 9, pp. 1711–1726, Sep. 2016.

[62] L. D. Brown, T. Cai, and A. DasGupta, "Confidence intervals for a binomial proportion and asymptotic expansions," *Ann. Statist.*, vol. 30, no. 1, pp. 160–201, 2002.

[63] M. Razzaghpour, R. Adeogun, I. Rodriguez, G. Berardinelli, R. S. Mogensen, T. Pedersen, P. Mogensen, and T. B. Sorensen, "Short-range UWB wireless channel measurement in industrial environments," in *Proc. Int. Conf. Wireless Mobile Comput., Netw. Commun. (WiMob)*, Oct. 2019, pp. 1–6.

[64] T. Olofsson, A. Ahlen, and M. Gidlund, "Modeling of the fading statistics of wireless sensor network channels in industrial environments," *IEEE Trans. Signal Process.*, vol. 64, no. 12, pp. 3021–3034, Jun. 2016.

[65] G. W. O. da Costa, A. F. Cattoni, I. Z. Kovacs, and P. E. Mogensen, "A scalable spectrum-sharing mechanism for local area network deployment," *IEEE Trans. Veh. Technol.*, vol. 59, no. 4, pp. 1630–1645, May 2010.

[66] A. Adouane, L. Rodier, K. Khawam, J. Cohen, and S. Tohme, "Game theoretic framework for inter-cell interference coordination," in *Proc. IEEE Wireless Commun. Netw. Conf. (WCNC)*, Apr. 2014, pp. 57–62.

[67] R. O. Adeogun, "A novel game theoretic method for efficient downlink resource allocation in dual band 5G heterogeneous network," *Wireless Pers. Commun.*, vol. 101, no. 1, pp. 119–141, Jul. 2018.

[68] J. Ellenbeck, C. Hartmann, and L. Berlemann, "Decentralized inter-cell interference coordination by autonomous spectral reuse decisions," in *Proc. 14th Eur. Wireless Conf.*, Jun. 2008, pp. 1–7.

[69] R. O. Adeogun, "Joint resource allocation for dual—Band heterogeneous wireless network," in *Proc. IEEE Wireless Commun. Netw. Conf. (WCNC)*, Apr. 2018, pp. 1–5.

[70] S. Li, S. C. Lay, W. H. Yu, and L. Wang, "Minimizing interference in mobile communications using genetic algorithms," in *Proc. Int. Conf. Comput. Sci.*, 2002, pp. 960–969.

[71] K. Tsagkaris, A. Katidiotis, and P. Demestichas, "Neural network-based learning schemes for cognitive radio systems," *Comput. Commun.*, vol. 31, no. 14, pp. 3394–3404, Sep. 2008.

[72] C. U. Castellanos, D. L. Villa, C. Rosa, K. I. Pedersen, F. D. Calabrese, P.-H. Michaelsen, and J. Michel, "Performance of uplink fractional power control in UTRAN LTE," in *Proc. IEEE Veh. Technol. Conf.*, May 2008, pp. 2517–2521.

[73] G. Miao and G. Song, *Energy and Spectrum Efficient Wireless Network Design*. Cambridge, U.K.: Cambridge Univ. Press, 2014.

[74] R. Adeogun, G. Berardinelli, I. Rodriguez, P. E. Mogensen, and M. Razzaghpour, "Measurement and analysis of radio frequency interference in the UWB spectrum," in *Proc. IEEE 90th Veh. Technol. Conf. (VTC-Fall)*, Sep. 2019, pp. 1–5.

[75] K. Siwiak, "Ultra-wideband radio," in *Encyclopedia of RF and Microwave Engineering*. Hoboken, NJ, USA: Wiley, 2005.

[76] R. Adeogun, G. Berardinelli, P. E. Mogensen, and I. Rodriguez, "Statistical characterization of wireless interference signal based on UWB spectrum sensing," in *Proc. IEEE Veh. Technol. Conf. (VTC Spring)*, May 2020, pp. 1–5.

[77] *Technical Requirements Applicable to all UWB Devices*, document 47 (CFR 47), 15.521, Code of Federal Regulations, FCC, 2005.

[78] *Short Range Devices (SRD) using Ultra Wide Band (UWB); Technical Characteristics for SRD Equipment Using Ultra Wide Band Sensor Technology (UWB) Based on Amended Mitigation Techniques for UWB*, document EN 103 314 (V1.1.1) (05-2017), ETSI, 2017.

[79] E. Karapistoli, F. Pavlidou, I. Gragopoulos, and I. Tsetsinas, "An overview of the IEEE 802.15.4a Standard," *IEEE Commun. Mag.*, vol. 48, no. 1, pp. 47–53, Jan. 2010.

[80] M. Tuchler, V. Schwarz, and A. Huber, "Location accuracy of an UWB localization system in a multi-path environment," in *Proc. IEEE Int. Conf. Ultra-Wideband*, Sep. 2005, pp. 414–419.

RAMONI ADEOGUN (Senior Member, IEEE) received the B.Eng. degree in electrical and computer engineering from the Federal University of Technology, Minna, Nigeria, and the Ph.D. degree in electronic and computer systems engineering from the Victoria University of Wellington, New Zealand. He is currently a Postdoctoral Fellow with Aalborg University, Denmark. Prior to joining Aalborg University, he has also worked in various positions at University of Cape Town, South Africa, Odua Telecoms Ltd., and the National Space Research and Development Agency, Nigeria. His research interests include channel characterization, machine learning and AI for communications, radio resource allocation, intelligent spectrum access, and interference management.

GILBERTO BERARDINELLI (Member, IEEE) received the first and second level degrees (*cum laude*) in telecommunication engineering from the University of L'Aquila, Italy, in 2003 and 2005, respectively, and the Ph.D. degree from Aalborg University, Denmark, in 2010. He is currently an Associate Professor with the Wireless Communication Networks (WCN) Section, Aalborg University, and also working in tight cooperation with Nokia Bell Labs. He is the author or coauthor of more than 100 international publications, including conference proceedings, journal contributions, and book chapters. His research interests include mostly focused on physical layer, medium access control, and radio resource management design for 5G systems.

PREBEN E. MOGENSEN received the M.Sc. and Ph.D. degrees from Aalborg University, in 1988 and 1996, respectively. Since 1995, he has been a part-time associated with Nokia in various research positions and have made contributions from 2G to 5G cellular technologies. He has been with Aalborg University, since graduation in 1988. In 2000, he became a Full Professor with Aalborg University, where he is currently leading the Wireless Communication Networks Section, Department of Electronic Systems. He is also a Principal Scientist with the Standardization Research Lab, Nokia Bell Labs. He has coauthored over 400 articles in various domains of wireless communication, and his Google Scholar H-index is 63. His current research interests include industrial use cases for 5G, 5G evolution, and 6G. He is a Bell Labs Fellow.

IGNACIO RODRIGUEZ (Member, IEEE) received the B.Sc. and M.Sc. degrees in telecommunication engineering from the University of Oviedo, Spain, and the M.Sc. degree in mobile communications and the Ph.D. degree in wireless communications from Aalborg University, Denmark. Since December 2016, he has been a Postdoctoral Researcher with Aalborg University. He is currently an External Research Engineer with Nokia Bell Labs, where he is mainly involved in 3GPP and ITU-R standardization activities. His research interests are mainly related to radio propagation, channel modeling, radio network planning and optimization, ultra-reliable and low-latency communications, and industrial IoT. He was a co-recipient of the IEEE VTS 2017 Neal Shepherd Memorial Best Propagation Paper Award, and in 2019, he was co-awarded with the 5G-prize by the Danish Energy Agency and the Danish Society of Telecommunication Engineers.

MOHAMMAD RAZZAGHPOUR (Member, IEEE) received the B.Sc. degree in electrical engineering from the University of Zanjan, Iran, in 2010, and the M.Sc. degree in electrical engineering from the K. N. Toosi University of Technology, Tehran, Iran, in 2014. He has a broad work experience in the telecommunication industry at Telecommunication Company of Iran (TCI) and Mobile Communication Company of Iran (MCCI). He is currently active as a Ph.D. Fellow with the Wireless Communication Network Section, Department of Electronic Systems, Aalborg University, Denmark. His research interests include the IIoT, LPWAN, WIRT, URLLC, and 6G.

• • •